A nonlinear model for the subgrid timescale experienced by heavy particles in large eddy simulation of isotropic turbulence with a stochastic differential equation

2013 New J. Phys. 15 035011

(http://iopscience.iop.org/1367-2630/15/3/035011)

New Journal of Physics
The open access journal for physics

A nonlinear model for the subgrid timescale experienced by heavy particles in large eddy simulation of isotropic turbulence with a stochastic differential equation

Guodong Jin and Guo-Wei He[1]
LNM, Institute of Mechanics, Chinese Academy of Sciences, Beijing 100190, People's Republic of China
E-mail: hgw@lnm.imech.ac.cn

New Journal of Physics **15** (2013) 035011 (27pp)
Received 6 August 2012
Published 11 March 2013
Online at http://www.njp.org/
doi:10.1088/1367-2630/15/3/035011

Abstract. The effects of subgrid scale (SGS) motions on the dispersion of heavy particles raise a challenge to the large-eddy method of simulation (LES). As a necessary first step, we propose the use of a stochastic differential equation (SDE) to represent the SGS contributions to the relative dispersions of heavy particles in LES of isotropic turbulence. The main difficulty is in closing the SGS-SDE model whilst accounting for the effects of particle inertia, filter width and gravity. The physics of the interaction between heavy particles and SGS turbulence is explored using the filtered direct numerical simulation method. It is found in the present work that (i) the ratio of the SGS Lagrangian and Eulerian timescales is different from that of the full-scale Lagrangian and Eulerian timescales. The ratios are also dependent on filter widths. (ii) In the absence of gravity, the SGS timescale seen by heavy particles non-monotonically changes with particle Stokes number and has a maximum at particle Stokes number ($St = \tau_p/\delta T_E$) near 0.5. (iii) In the presence of gravity, a similarity law exists between the SGS Lagrangian correlation function seen by a heavy particle within a time-delay τ and the SGS spatial correlation function with the displacement $\langle w\rangle\tau$, where $\langle w\rangle$ is the average settling velocity of a heavy particle. The joint effects of particle inertia and gravity are accounted for using the elliptic model for pair

[1] Author to whom any correspondence should be addressed.

correlation of SGS velocity seen by heavy particles. The SGS timescale seen by heavy particles is extracted from the elliptic model and used to close the SGS-SDE model. The validations of the model against direct numerical simulation show that the SGS-SDE model can improve the performance of LES on relative dispersions especially when their initial separations are in the inertial subrange. Furthermore, we assess the performance of the SGS-SDE model by comparing the results with the approximate deconvolution method. The results show that the SGS-SDE model is more suitable for particles with small Stokes numbers, $St_K < 2$. The model developed here provides a basis for the development of a more advanced SGS model for particles in non-homogeneous and anisotropic turbulent flows in pipes or channels.

Contents

1. Introduction **2**
2. The governing equations and timescales of fluid motions **4**
2.1. Equations for isotropic turbulent flows 4
2.2. Equations for particle motion 6
2.3. The subgrid scale stochastic model for a heavy particle in large-eddy simulation 6
2.4. Subgrid scale timescale seen by heavy particles 7
3. Closure for the subgrid scale stochastic model **8**
3.1. Eulerian and Lagrangian timescales at full scale and subgrid scale 8
3.2. Inertial effects on the subgrid scale timescale seen by heavy particles 12
3.3. The elliptic model for the subgrid scale timescale seen by heavy particles under gravity 14
4. Large-eddy simulation of two-particle relative dispersion **18**
4.1. Validation of the subgrid scale-stochastic differential equation model by comparison with direct numerical simulation 18
4.2. Assessment of the subgrid scale-stochastic differential equation model by comparing with the approximate deconvolution methods 21
5. Conclusions and future work **24**
Acknowledgments **25**
References **25**

1. Introduction

Particle-laden turbulent flows can be found in a wide range of engineering and environmental flow problems [1]. For example, pollutant dispersion and warm rain droplet formation in the atmosphere, and fluidization and combustion in process engineering [2–4]. Understanding the relative dispersion of heavy particles in turbulence is vital for the processes of transport and mixing, since it is closely related to the fluctuation of local concentration, which determines reaction rates [5–8].

When turbulent flows are simulated using the Reynolds average numerical simulation (RANS) method and the heavy particles are tracked using the Lagrangian method, stochastic differential equations (SDE) are usually used to represent the contributions of turbulent

fluctuations to the dispersion of particles [9, 10]. Chibbaro and Minier [10] addressed the importance of introducing specific features related to the near-wall coherent structure in pipe flows based on the Langevin probability density function (PDF) method. In the SDE, the Lagrangian integral timescale of fluid velocity seen by heavy particles (the fluid–particle interaction timescale), T_{Lp}, is one of the key parameters and it determines the dispersion rates of heavy particles [11–14]. Direct numerical simulation (DNS) shows that T_{Lp} does not vary monotonically with particle Stokes number St_{K} from T_{L} to T_{E}, but has an 'N' shape with a maximum near $St_{\mathrm{K}} = 1$ due to the relative motion of particles near rotational vortical structures [15–17], where $St_{\mathrm{K}} \equiv \tau_{\mathrm{p}}/\tau_{\mathrm{K}}$, τ_{p} is the particle Stokes response time and $\tau_{\mathrm{p}} = \rho_{\mathrm{p}} d_{\mathrm{p}}^2/18\mu$, d_{p} is the particle diameter, μ the dynamical viscosity, ρ_{p} particle density and τ_{K} the turbulent Kolmogorov timescale.

The RANS method finds wide application in engineering calculations [9] and the DNS method has manifested its power in fundamental research [17–20]. However, DNS is still limited to flows at relatively low or moderate Reynolds numbers. RANS does not predict well the unsteady structures in turbulent flows which are of importance for turbulent dispersion of heavy particles. Motivated by the limitations of RANS and DNS, large-eddy simulation (LES) is becoming a potential method for future engineering calculations. In LES, large-scale velocities $\bar{\boldsymbol{u}}(\boldsymbol{x}, t)$ are resolved explicitly using the filtered Navier–Stokes equations. The small-scale velocities $\boldsymbol{u}'(\boldsymbol{x}, t)$ are ignored but their effects on large-scale velocities are modeled using an subgrid scale (SGS) model [21–25].

If one uses the resolved large-scale velocity $\bar{\boldsymbol{u}}(\boldsymbol{x}, t)$ to replace the real fluid velocity $\boldsymbol{u}(\boldsymbol{x}, t)$ and calculates the particle motion with the SGS velocity being neglected, large errors in the statistics related to both fluid particles and inertial particles can be observed [26–31]. The effects of SGS fluid motions on the dynamics of particles are an important and open issue. In isotropic turbulence, the relative dispersion of heavy particles is mainly dominated by small-scale fluid motions. In channel flows, complex flow structures exist due to the mean shear rate and the anisotropy near the wall. Thus the relative dispersions are controlled by the wall-dependent flow structures. Marchioli *et al* [27] verified the important effect of subgrid turbulence on particle motions and tried to explicitly recover SGS effects using fractal interpolation and approximate deconvolution methods (ADM). They further pointed out the necessity to introduce the information of flow structures to quantitatively predict particle segregation and preferential concentration [28]. Jin *et al* [31], and more recently Bianco *et al* [32], studied the effects of the filtering errors on particle clustering in isotropic turbulence and channel flows, respectively. In the latter, the filtering error is a function of the wall distance and has a maximum in the buffer region. Many other efforts have been devoted to this issue, using the ADM [28, 33–38], stochastic models [39–47] and fractal interpolation [28]. The ADM is favorable to correct the resolved eddies near cutoff scales but cannot be used to recover the ones below the cutoff scales. Therefore, the SDE model becomes the favored candidate and we shall assess the performances of the SGS-SDE model and the ADM by comparing their prediction results.

The SGS timescale seen by heavy particles is a key parameter for the closure of the SGS-SDE model which describes the interaction timescale between heavy particles and SGS eddies. Shotorban and Mashayek [39] and Fede *et al* [41] assumed that the SGS timescale δT_{Lp} seen by heavy particles is equal to the Lagrangian integral timescale of SGS fluid velocity δT_{L}, that is, $\delta T_{\mathrm{Lp}} = \delta T_{\mathrm{L}}$. The assumption is only suitable for particles with very small Stokes numbers. Berrouk *et al* [42, 43] proposed a model for the timescale in the SGS-SDE model using the Wang–Stock model [11] to consider heavy particle dispersion in LES. Jin *et al* [46] proposed a

model for the dependence of δT_{Lp} on the Stokes number and filter width in isotropic turbulence. Geurts and Kuerten [48] analyzed the characters of the SGS stochastic force acting on particles in turbulent channel flow. However, the effects of the drift velocity due to gravity were not considered. Under gravity, the crossing trajectory effect [14] reduces the interaction timescale between SGS turbulent eddies and heavy particles in the context of LES. In LES, the drift velocity effect is important when the particle drift velocity is comparable to the root mean square (rms) turbulent velocity. Therefore, the effects of drift velocity on the SGS timescale seen by heavy particles require further investigation.

As a necessary first step to more complex wall-bounded turbulent flows, the purpose of this paper is to investigate the closure for the SGS-SDE model, *especially* to provide the SGS timescale seen by particles *with a mean drift velocity* in isotropic turbulent flows. The results obtained provide a basis for constructing more advanced models for LES of inhomogeneous and anisotropic turbulent flows such as channel or pipe flows.

The paper is organized as follows. The governing equations for fluid and particle motions and the definitions of integral timescales of fluid velocities at full- and SGSs are given in section 2. The difference between the Lagrangian and Eulerian timescales at full- and SGSs, the non-monotonical variations of the SGS timescale seen by heavy particles and the elliptic model for the SGS particle–fluid timescale under consideration of drift velocity are given in section 3. The validation of the proposed SGS-SDE model for relative dispersion and the comparison between the performances of the SGS-SDE model and the ADM are given in section 4. The conclusions and proposals for future work are presented in section 5.

2. The governing equations and timescales of fluid motions

In the turbulent flow simulated, particle concentration is very dilute and particle diameter d_{p} is smaller than the Kolmogorov lengthscale η, thus one-way coupling is assumed. The equations for turbulent flows and particle motions are described in this section.

2.1. Equations for isotropic turbulent flows

2.1.1. Direct numerical simulation method. In spectral space, the Navier–Stokes equation for the isotropic and incompressible turbulence in a box of $(2\pi)^3$ can be represented as ($k < k_{\max}$)

$$\left(\frac{\partial}{\partial t} + \nu k^2\right) \hat{\boldsymbol{u}}(\boldsymbol{k}, t) = \boldsymbol{P}(\boldsymbol{k}) \mathcal{F}(\boldsymbol{u} \times \boldsymbol{\omega}) + \hat{\mathbf{f}}(\boldsymbol{k}, t), \tag{1}$$

where $\hat{\boldsymbol{u}}(\boldsymbol{k}, t)$ is a Fourier coefficient, $\boldsymbol{k} = (k_x, k_y, k_z)$ the wavenumber vector and $k = |\mathbf{k}|$, $\boldsymbol{u}$ and $\boldsymbol{\omega}$ fluid velocity and vorticity in physical space, ν fluid kinematical viscosity. $\mathcal{F}$ denotes a Fourier transform, $\boldsymbol{P}_{jm} = \delta_{jm} - k_j k_m / k^2$ ($j, m = 1, 2, 3$). The random artificial force $\hat{\mathbf{f}}(\boldsymbol{k}, t)$ proposed by Eswaran and Pope [49] is used to drive and maintain the turbulent flow. The random force is a vector-valued Uhlenbeck–Ornstein stochastic process. It is characterized by three parameters, the forcing radius $0 < \|\mathbf{k}\| < \sqrt{8}$, the forcing amplitude $\sqrt{447.3}$ and a timescale of 0.038.

The flow domain is discretized uniformly into N^3 grid points ($N = 256$ in this paper). The maximum cutoff wavenumber $k_{\max} = N/3$. The Fourier coefficients are advanced in time using a second-order Adams–Bashforth method for the nonlinear term and an exact integration for the linear viscous term. The time step is chosen to ensure that the Courant–Friedrichs–Lewy number is 0.5 or less for numerical stability and accuracy [18].

2.1.2. Filtered-DNS method. The filtered velocity field is calculated from the Fourier coefficients obtained from DNS using a sharp spectral filter $H(k_c - |\boldsymbol{k}|)$ (H is the Heaviside function)

$$\tilde{\boldsymbol{u}}(\boldsymbol{x}, t) = F^{-1} \begin{cases} \hat{\boldsymbol{u}}(\boldsymbol{k}, t) & \text{if } |k| \in [1, k_c], \\ 0 & \text{if } |k| \in (k_c, k_{max}], \end{cases} \tag{2}$$

where $\tilde{\boldsymbol{u}}(\boldsymbol{x}, t)$ is the filtered velocity in physical space, k_c the cutoff wavenumber. The subgrid velocity field is then

$$\boldsymbol{u}'(\boldsymbol{x}, t) = \boldsymbol{u}(\boldsymbol{x}, t) - \tilde{\boldsymbol{u}}(\boldsymbol{x}, t). \tag{3}$$

One of the advantages of FDNS is that the full-scale turbulent flow field from DNS is directly decomposed into a large-scale part and a small-scale part using equations (2) and (3). Thus, we can study the characteristics of the SGS flow field and the interaction between heavy particles and SGS motions directly. By varying the cutoff wavenumber k_c, we can study the effects of filter width on the SGS timescale seen by heavy particles.

2.1.3. Large-eddy simulation method. The LES of isotropic turbulence is performed on the coarser grids using the same pseudo-spectral method and large-scale forcing scheme as DNS. The governing equation in LES is given by ($k \leqslant k_c$, k_c is the cutoff wavenumber in LES)

$$\left\{ \frac{\partial}{\partial t} + [\nu + \nu_e(k|\, k_c)]k^2 \right\} \hat{\bar{\boldsymbol{u}}}(\boldsymbol{k}, t) = \boldsymbol{P}(\boldsymbol{k}) F(\bar{\boldsymbol{u}} \times \bar{\boldsymbol{\omega}}) + \hat{\boldsymbol{f}}(\mathbf{k}, t), \tag{4}$$

where $\bar{\boldsymbol{u}}$ and $\bar{\boldsymbol{\omega}}$ are the resolved velocity and vorticity in physical space respectively. The term $\nu_e(k|\, k_c)k^2\hat{\bar{\boldsymbol{u}}}(\boldsymbol{k}, t)$ on the left-hand side represents the net effects of SGS motions on the resolved ones. The spectral SGS eddy viscosity model [50, 51] is used,

$$\nu_e(k|\, k_c) = \nu_e^+(k/k_c)\sqrt{\frac{E(k_c)}{k_c}} \tag{5}$$

with

$$\nu_e^+(k/k_c) = C_K^{-3/2}[0.441 + 15.2\, \exp(-3.03k_c/k)]. \tag{6}$$

The spectral viscosity $\nu_e(k|\, k_c)$ depends on the wavenumber k, k_c and $E(k_c)$, the value of the energy spectrum function at k_c. Here, $E(k_c)$ in equation (5) is dynamically evaluated from the LES fluid field. The Kolmogorov constant C_K has a universal value at an asymptotically high Reynolds number [52, 53]. To be consistent with the flow obtained from the DNS, $C_K = 2.1$ is obtained by fitting the compensated spectrum in DNS; it is a bit larger than the experimental value $C_K = 1.62$ [54] due to the modest Reynolds number in this study. The same value was used by Chasnov [55] in the LES of Kolmogorov inertial subrange.

If we neglect the numerical error by virtue of the spectral method, there are filtering errors and SGS modeling errors in real LES. The filtering error comes from the absence of SGS velocity due to the filtering operation [32]. The modeling error comes from the fact that the LES only gives an approximation and cannot provide the same filtered velocity as FDNS due to the limitations of currently available SGS models [34]. The SGS eddy viscosity model is usually too dissipative and it alters the local flow structure and timescales of resolved scales. The changes in the resolved flow structures in LES lead to a larger integral timescale of the velocity correlation functions [26] and a slower dispersion rate than that in FDNS, which will be seen in section 4.

2.2. Equations for particle motion

The discrete phase is composed of 400 000 solid, spherical particles with diameter $d_p = 0.5\eta$ and $\rho_p/\rho_f \gg 1$ where ρ_f is the fluid density. Many forces act on a single particle suspended in a turbulent flow field [56]. Since $\rho_p/\rho_f \gg 1$, the forces on a small particle can be simplified as drag force and gravity force. Then, the governing equations for a single particle can be written as

$$\frac{\mathrm{d}\boldsymbol{x}_p(t)}{\mathrm{d}t} = \boldsymbol{v}_p(t), \tag{7}$$

$$\frac{\mathrm{d}\boldsymbol{v}_p(t)}{\mathrm{d}t} = \frac{(\boldsymbol{u}(\boldsymbol{x}_p(t), t) - \boldsymbol{v}_p(t))f + \boldsymbol{w}_0}{\tau_p}, \tag{8}$$

where $\boldsymbol{x}_p(t)$ and $\boldsymbol{v}_p(t)$ are the particle position and velocity at time t, $\boldsymbol{w}_0$ the particle Stokes settling velocity in a still fluid under gravitational acceleration, $\mathbf{g}$ and $\boldsymbol{w}_0 = \mathbf{g}\tau_p$. $\boldsymbol{u}(\boldsymbol{x}_p(t), t)$ is the fluid velocity seen by a particle. The velocity is obtained from the flow field by a three-dimensional (3D) six-point Lagrangian interpolation scheme [18], f is the nonlinear drag correction coefficient,

$$f(Re_p) = 1 + 0.15Re_p^{0.687}, \tag{9}$$

which is determined by the instantaneous value of the particle Reynolds number

$$Re_p = \left|\boldsymbol{u} - \boldsymbol{v}_p\right| d_p/\nu. \tag{10}$$

Letting $\boldsymbol{u} = 0$, $v_p = \langle w \rangle$ and $\mathrm{d}\boldsymbol{v}_p(t)/\mathrm{d}t = 0$ in equation (8), we can obtain the relation between the real average settling velocity $\langle w \rangle$ and the Stokes settling velocity $w_0 = g\tau_p$ from equations (9) and (10) in a still fluid as

$$w_0 = \langle w \rangle \left(1 + 0.15\left(\frac{d_p\langle w \rangle}{\nu}\right)^{0.687}\right), \tag{11}$$

$\langle w \rangle$ is a necessary parameter for the closure of the SGS-SDE model in the presence of gravity in equations (46) and (47). Equation (11) is used to account for the nonlinear effects of particle Reynolds number on particle settling velocity. We can quickly estimate the particle Reynolds number if we assume that the average relative velocity between fluid and particle is about the fluid rms fluctuating velocity 19.34, particle diameter is $0.5\eta = 0.006\,75$, fluid kinematical viscosity $\nu = 0.0488$, then $Re_p = 1.48$.

The motion of a particle is obtained by numerical integration of equations (7) and (8) using a fourth-order Adams–Bashforth method for the particle velocity and a fourth-order Adams–Moulton method for particle trajectory, respectively.

2.3. The subgrid scale stochastic model for a heavy particle in large-eddy simulation

Following the ideas of Simonin *et al* [9] and Pope [57], we propose an SGS-SDE model for the SGS velocity seen by heavy particles in the context of the LES of heavy particles. The full-scale fluid velocity seen by a heavy particle is then modeled as

$$\mathrm{d}u_i^+ = \left\{\bar{u}_i\left[x_p(t + \mathrm{d}t), t + \mathrm{d}t\right] - \bar{u}_i\left[x_p(t), t\right]\right\} - \frac{1}{\delta T_{\mathrm{Lp},ii}}(u_i^+ - \bar{u}_i)\mathrm{d}t + (C_i\varepsilon_{\mathrm{SGS}}\,\mathrm{d}t)^{1/2}\,\xi, \tag{12}$$

where the superscript + in equation (12) denotes the modeled full-scale velocity. The first term on the right-hand side is taken from the resolved velocity in the LES, the second and the third terms constitute a Langevin equation. ξ is a Gaussian random variable of zero mean and unit variance, the timescale of the Lagrangian correlation function of the SGS velocity seen by heavy particles (we shall simply call $\delta T_{\mathrm{Lp,ii}}$ the SGS timescale seen by heavy particles hereinafter) and the coefficient C_i depend on the direction of velocity u_i^+ along or vertical to gravity (please see equations (46)–(48) for $\delta T_{\mathrm{Lp,ii}}$ and C_i in section 3.3) [58]. In equation (12), the SGS dissipation rate $\varepsilon_{\mathrm{SGS}}$ is evaluated in spectral space as

$$\varepsilon_{\mathrm{SGS}} = 2\int_1^{k_c} \nu_e(k|\,k_c)k^2E(k)\,\mathrm{d}k. \tag{13}$$

The second term on the right-hand side of equation (12) represents the memory of the SGS velocity seen by a particle at the previous time step and the third term accounts for the contribution of SGS fluctuations seen by heavy particles.

In order to close equation (12), we need to specify $\delta T_{\mathrm{Lp,ii}}$ and C_i considering the particle inertia, filter width and the effects of gravity. We shall firstly give the definitions of the correlation functions and the timescales at full- and SGSs used in this paper.

2.4. Subgrid scale timescale seen by heavy particles

The Eulerian temporal correlation can be calculated as

$$R_{\mathrm{E},ij}(\tau) = \frac{\langle u_i(\boldsymbol{x}, t_0)u_j(\boldsymbol{x}, t_0+\tau)\rangle}{\langle u_i(\boldsymbol{x}, t_0)u_j(\boldsymbol{x}, t_0)\rangle} \tag{14}$$

and the Eulerian integral timescale is then

$$T_{\mathrm{E},ij} = \int_0^\infty R_{\mathrm{E},ij}(\tau)\mathrm{d}\tau, \tag{15}$$

where $i, j = 1, 2, 3$ denote the directions of the three axes. The Lagrangian correlation can be calculated as

$$R_{\mathrm{L},ij}(\tau) = \frac{\langle u_i(\boldsymbol{x}_0, t_0)u_j(\boldsymbol{x}(t_0+\tau), t_0+\tau)\rangle}{\langle u_i(\boldsymbol{x_0}, t_0)u_j(\boldsymbol{x_0}, t_0)\rangle} \tag{16}$$

and the Lagrangian integral timescale is

$$T_{\mathrm{L},ij} = \int_0^\infty R_{\mathrm{L},ij}(\tau)\mathrm{d}\tau. \tag{17}$$

The SGS Eulerian temporal correlation can be calculated as

$$\delta R_{\mathrm{E},ij}(\tau) = \frac{\langle u_i'(\boldsymbol{x}, t_0)u_j'(\boldsymbol{x}, t_0+\tau)\rangle}{\langle u_i'(\boldsymbol{x}, t_0)u_j'(\boldsymbol{x}, t_0)\rangle} \tag{18}$$

and SGS Eulerian integral timescale is

$$\delta T_{\mathrm{E},ij} = \int_0^\infty \delta R_{\mathrm{E},ij}(\tau)\mathrm{d}\tau. \tag{19}$$

The SGS Lagrangian correlation can be calculated as

$$\delta R_{\mathrm{L},ij}(\tau) = \frac{\langle u_i'(\boldsymbol{x}_0, t_0)u_j'(\boldsymbol{x}(t_0+\tau), t_0+\tau)\rangle}{\langle u_i'(\boldsymbol{x_0}, t_0)u_j'(\boldsymbol{x_0}, t_0)\rangle} \tag{20}$$

Table 1. Flow parameters in the DNS 256^3.

Method	DNS (256^3)
Reynolds number Re_λ	102.05
rms fluid velocity $u_{\rm rms}$	19.34
Dissipation rate ε	3554.4
Minimum lengthscale η	0.0135
Minimum timescale $\tau_{\rm K}$	0.0037
Minimum velocity scale $v_{\rm K}$	3.6272
Large-eddy turnover timescale $T_{\rm E}$	0.051
Lagrangian integral timescale $T_{\rm L}$	0.037
Integral lengthscale L_f	0.9946
Viscosity ν	0.0488

and SGS Lagrangian integral timescale is

$$\delta T_{{\rm L},ij} = \int_0^\infty \delta R_{{\rm L},ij}(\tau){\rm d}\tau. \tag{21}$$

Here it is important to point out that $\boldsymbol{x}(t_0+\tau)$ in equations (16) and (20) is the location of a fluid particle based on the full-scale velocity field

$$\frac{{\rm d}\boldsymbol{x}(t_0+\tau)}{{\rm d}\tau} = \boldsymbol{u}(\boldsymbol{x}(t_0+\tau), t_0+\tau). \tag{22}$$

The Lagrangian correlation function of the SGS velocity seen by heavy particles can be calculated as

$$\delta R_{{\rm Lp},ij}(\tau) = \frac{\left\langle u_i'(\boldsymbol{x}_{\rm p}(t_0), t_0)u_j'(\boldsymbol{x}_{\rm p}((t_0+\tau), t_0+\tau)\right\rangle}{\left\langle u_i'(\boldsymbol{x}_{\rm p}(t_0), t_0)u_j'(\mathbf{x}_{\rm p}(t_0), t_0)\right\rangle}, \tag{23}$$

where particle position $\boldsymbol{x}_{\rm p}((t_0+\tau), t_0+\tau)$ is obtained by solving equation (7). We shall simply call $\delta R_{{\rm Lp},ij}(\tau)$ the SGS correlation seen by heavy particles in this paper. The SGS timescale seen by heavy particles used in equation (12) can be calculated as

$$\delta T_{{\rm Lp},ij} = \int_0^\infty \delta R_{{\rm Lp},ij}(\tau){\rm d}\tau. \tag{24}$$

Without the force of gravity, the motions of both particles and fluid are isotropic and $\delta T_{{\rm Lp},ij}$ reduces to $\delta T_{\rm Lp}$.

3. Closure for the subgrid scale stochastic model

3.1. Eulerian and Lagrangian timescales at full scale and subgrid scale

Table 1 lists the flow parameters of the isotropic turbulent flow simulated in the present study. All the parameters in the table are non-dimensional. Figure 1 plots the energy spectrum from the DNS of isotropic turbulence on resolution of 256^3. Here the vertical dashed lines represent

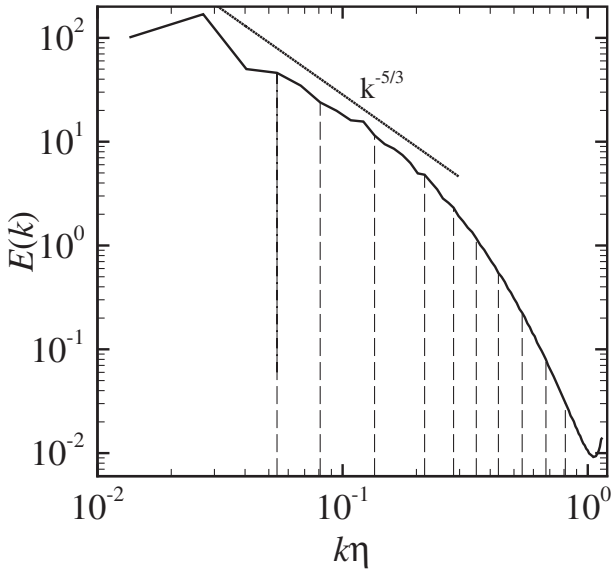

Figure 1. The energy spectrum of the simulated flow in DNS (256^3). The vertical dashed lines denote different cutoff locations in FDNS.

the different cutoff wavenumbers in FDNS. The rms velocity $u_{\rm rms}$ and average dissipation rate ε are defined below and computed from the energy spectrum as shown in figure 1

$$u_{\rm rms} = \sqrt{\frac{1}{3}\langle u_i u_i \rangle} = \sqrt{\frac{2}{3}\int_1^{k_{\rm max}} E(k)\,{\rm d}k}, \tag{25}$$

$$\varepsilon = \int_1^{k_{\rm max}} 2\nu k^2 E(k)\,{\rm d}k. \tag{26}$$

Therefore, the Kolmogorov length, time and velocity scales in DNS are defined as

$$\eta = (\nu^3/\varepsilon)^{0.25}, \quad \tau_{\rm K} = (\nu/\varepsilon)^{0.5}, \quad {\rm v}_{\rm K} = (\varepsilon\nu)^{0.25}. \tag{27}$$

For full-scale velocity in isotropic turbulent flows, the Eulerian velocity correlation $R_{\rm E}(\tau)$ from equation (14) decorrelates slower than its Lagrangian counterpart $R_{\rm L}(\tau)$ from equation (16), as shown in figure 2. Therefore, the Eulerian integral timescale is larger than its Lagrangian counterpart, $T_{\rm E} > T_{\rm L}$. Figure 3 shows that the ratio of Lagrangian integral timescale to the Eulerian integral timescale is independent of turbulent Reynolds number Re_λ and has a mean value of 0.78 [59]. Our current result is consistent with the previous results. The fact that the timescale ratio is less than one at full-scale is contrary to the results at SGSs which can be observed in figure 2.

A full-scale turbulent flow field can be directly decomposed into a large-scale part and an SGS part using the low-pass sharp spectral filter, see equation (2). The SGS flow field can be thus obtained using equation (3). Figure 4 shows the slices of vorticity contour obtained from the above decomposition at the cutoff wavenumber $k_{\rm c} = 21$ or $\eta k_{\rm c} = 0.284$ at $z = \pi$. Figure 4(a) shows the vorticity contour of the full-scale turbulent flow field $\boldsymbol{u}$. Figure 4(b) shows the vorticity contour of the large-scale part of the turbulent flow field $\tilde{\boldsymbol{u}}$, while figure 4(c) shows

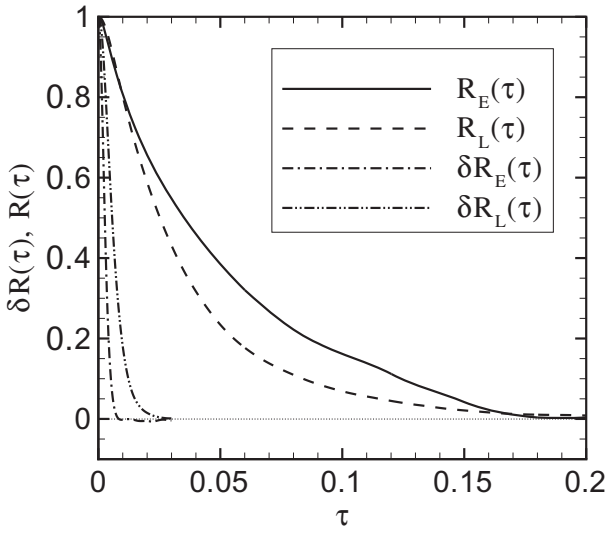

Figure 2. Eulerian and Lagrangian fluid velocity temporal correlation functions of the full-scale field and SGS field at $\eta k_c = 0.284$. In contrast to the full-scale flow field case, the SGS Eulerian temporal correlation decorrelates faster than its Lagrangian counterpart in SGS flow field since the small-scale eddies are convected by energy-containing large eddies in turbulence.

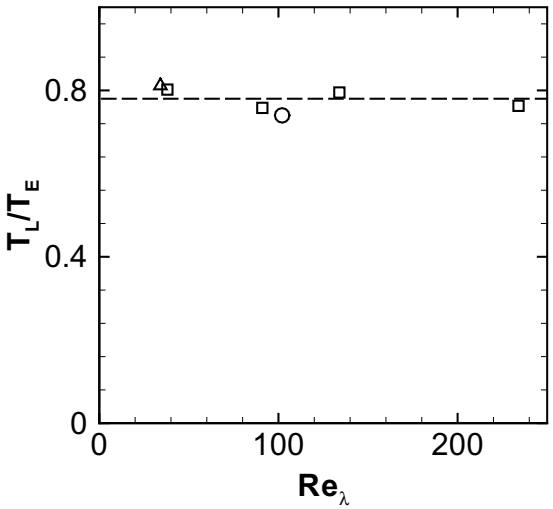

Figure 3. The ratio of Lagrangian integral timescale to Eulerian integral timescale at different Reynolds numbers. ○: present result; □: results from [59]; △: result from [16]; − − −−: the mean value 0.78 from [59]. It is observed that the ratio is independent of Reynolds number.

the vorticity contour of the small-scale (or SGS) part of the turbulent flow field $\boldsymbol{u}'$. It can be observed that the vorticity contour in figure 4(b) is much smoother than that in figure 4(a) due to the low-pass filtering operation. However, there are many small-scale structures with high vorticity in figure 4(c).

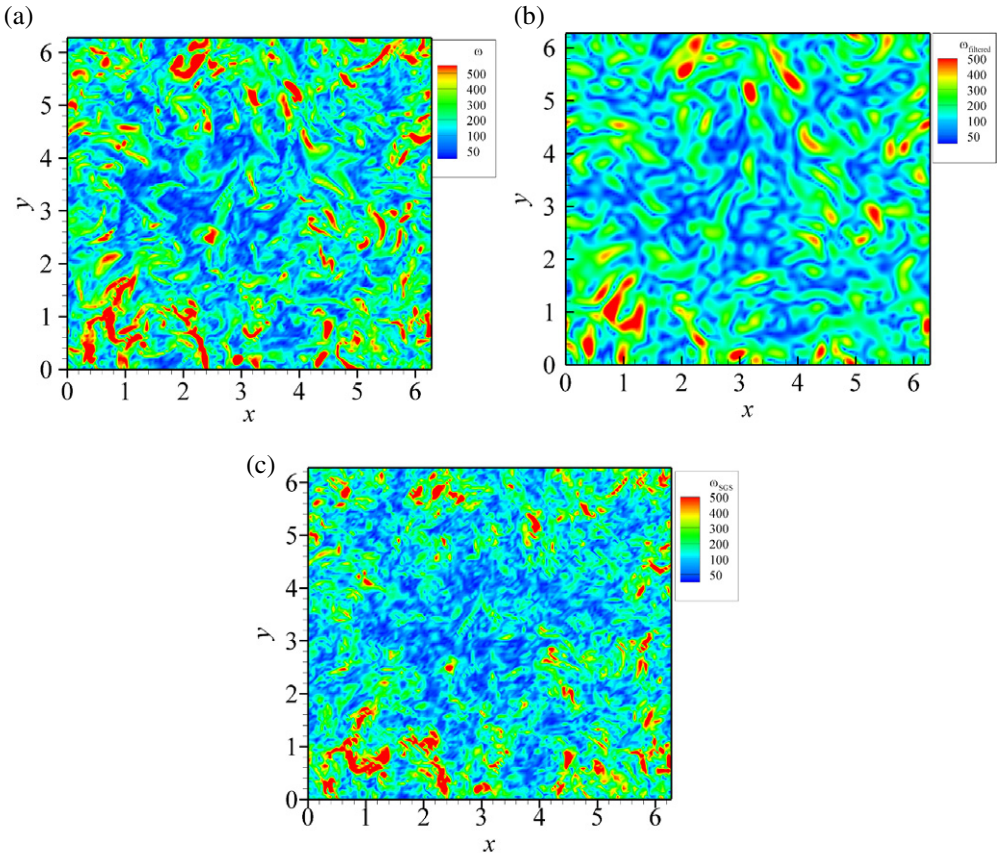

Figure 4. Vorticity contours of the full-scale flow field, filtered flow field and SGS flow field at $z = \pi$ in DNS 256^3, where $k_c = 21$ and $\omega_x = \tilde{\omega}_x + \omega'_x$, $\omega_y = \tilde{\omega}_y + \omega'_y$. The filtered field is smooth, while the SGS field exhibits many small-scale structures. (a) Full-scale vorticity contour $\sqrt{\omega_x^2 + \omega_y^2}$, (b) Filtered vorticity contour $\sqrt{\tilde{\omega}_x^2 + \tilde{\omega}_y^2}$ and (c) SGS vorticity contour $\sqrt{{\omega'_x}^2 + {\omega'_y}^2}$.

In contrast to the full-scale velocity field where the Eulerian velocity decorrelation rate is slower than its Lagrangian counterpart, the SGS Eulerian correlation function $\delta R_E(\tau)$ decorrelates faster than its Lagrangian counterpart $\delta R_L(\tau)$, as shown in figure 2, where the cutoff wavenumber is at $\eta k_c = 0.284$. This is because in a turbulent flow field, the Eulerian time correlation is dominated by the sweeping effect, the small-scale eddies in the SGS part are carried and convected by the large-scale velocity. Thus, the SGS Eulerian correlation function decorrelation rate is fast and the integral timescale δT_E is shorter than the SGS Lagrangian integral timescale δT_L. One additional observation from figure 2 is that both $\delta R_E(\tau)$ and $\delta R_L(\tau)$ decorrelate at much faster rates than $R_E(\tau)$ and $R_L(\tau)$, respectively. This is because the SGS field is 'more' *δ-correlated* than the full-scale field as shown in figures 4(a) and (c).

The SGS Lagrangian and Eulerian timescales and their ratio $\beta = \delta T_L / \delta T_E$ are necessary parameters for the model of the SGS timescale seen by inertial particles, see equation (31) for details. The SGS Eulerian timescale δT_E can be estimated using

$$\delta T_E = \frac{3\pi}{10} \frac{1}{k_c \bar{u}_{rms}}, \tag{28}$$

where $3\pi/10k_c$ is the SGS integral lengthscale (see equation (39) for details). $\bar{u}_{rms}$ is the rms of resolved fluctuating velocity in LES. The SGS Lagrangian timescale can be estimated using

$$\delta T_L = \frac{1}{0.5 + 0.75C_0} \frac{k_{SGS}}{\varepsilon_{SGS}}, \tag{29}$$

where C_0 is a constant and it is closely related to the Lagrangian Kolmogorov constant. However, there is great uncertainty about the numerical value of Lagrangian Kolmogorov constant and it varies in the range 2.0–7.0 estimated from DNS and experiments [57, 60]. A recent estimation of the Lagrangian Kolmogorov constant is about 6.9 ± 0.2 using DNS data at high Reynolds number [61]. Sheikhi *et al* [62] set C_0 to be 2.1 in the LES of a passive scalar using the SDE. As the extent of the consistency between the Langevin equation for a fluid particle and the Kolmogorov hypotheses about the second-order Lagrangian structure function is still an open question, we set $C_0 = 2.1$ in FDNS plus SDE and $C_0 = 6.0$ in LES plus SDE, respectively, in the present study. The SGS kinetic energy k_{SGS} in equation (29) can be estimated using

$$k_{SGS} = C_\varepsilon (\varepsilon_{SGS} \Delta)^{2/3} \tag{30}$$

and $C_\varepsilon = 1.0$ and the filter width in physical space $\Delta = \pi/k_c$. ε_{SGS} in equation (29) is calculated using equation (13) in the spectral space. The ratio $\beta = \delta T_L/\delta T_E$ is larger than unit at the SGS, this is expected if we observe the decorrelation rates of the SGS correlation functions in figure 2.

3.2. Inertial effects on the subgrid scale timescale seen by heavy particles

The particle inertia affects the SGS timescale seen by heavy particles. In the case of a particle with a finite Stokes number, the SGS Lagrangian correlation seen by a particle, $\delta R_{Lp}(\tau)$, in the absence of gravity is shown in figure 5, where the cutoff location is at $\eta k_c = 0.284$. It is observed in figure 5 that the behavior of $\delta R_{Lp}(\tau)$ changes within three limits: the SGS Lagrangian correlation at $St \sim 0$ ($St = \tau_p/\delta T_E$), the SGS Eulerian correlation at $St \sim \infty$ and a strongest correlation at $St \sim 0.5$. Among the three limits, there are two regimes: for $0 < St \leqslant 0.5$, the correlation $\delta R_{Lp}(\tau)$ decays more slowly with increasing St as shown in figure 5(a); for $St > 0.5$, the correlation $\delta R_{Lp}(\tau)$ decays faster and faster with increasing St and finally approaches the SGS Eulerian correlation, as shown in figure 5(b). Similar behavior of full-scale velocity seen by heavy particles in an isotropic turbulent flow field was previously observed by Jung *et al* [17].

Quantitatively, the variation of SGS timescale seen by heavy particles, δT_{Lp}, is obtained by integrating $\delta R_{Lp}(\tau)$ from 0 to ∞ and is shown in figure 6 using circles. As discussed above, our DNS results show that for $St < 0.03$, $\delta T_{Lp} \approx \delta T_L$ or the difference between δT_L and δT_{Lp} is negligible. Particles with very large Stokes numbers, $St \approx 100$ or larger, do not respond to the SGS eddies, thus $\delta T_{Lp} \to \delta T_E$. For a particle with intermediate Stokes number, $\delta T_{Lp}/\delta T_L$ varies with St and this variation is *non-monotonic*. The ratio $\delta T_{Lp}/\delta T_L$ first increases with increasing St, reaches a maximum at $St \sim 0.5$ and then decreases to approach the limiting value of $\delta T_E/\delta T_L$. Our numerical results can be fitted by an empirical curve (solid line in figure 6) [46]

$$\frac{\delta T_{Lp}}{\delta T_L} = \frac{1}{\beta}\left\{(0.444 - 0.7\eta k_c)\exp\left\{-\left[\ln\left(\frac{St}{0.5}\right)\right]^2\right\} + 1 - (1-\beta)\exp\left(-\frac{St}{5.15}\right)\right\}, \tag{31}$$

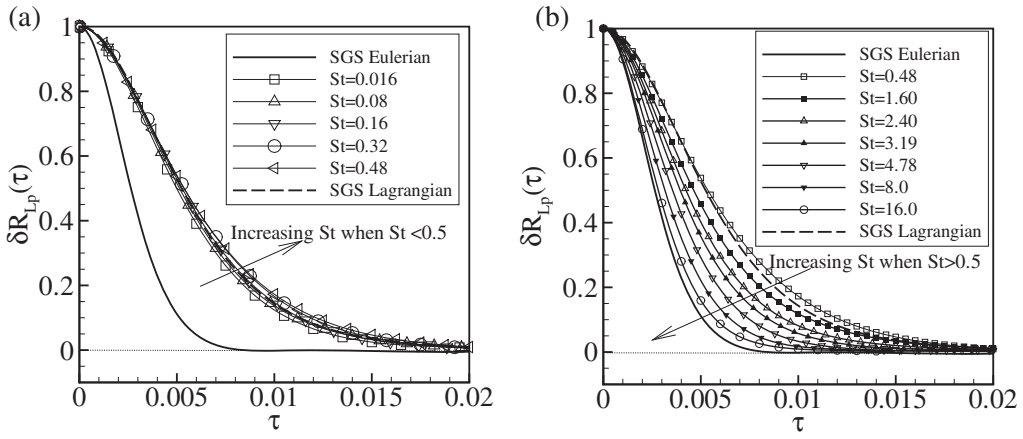

Figure 5. Lagrangian correlation functions of SGS fluid velocity seen by heavy particles, $\eta k_c = 0.284$. (a) $St \leqslant 0.5$, the correlation function increases with particle Stokes numbers, $St = \tau_p/\delta\tau_E$. (b) $St > 0.5$, the correlation function decreases with particle Stokes numbers.

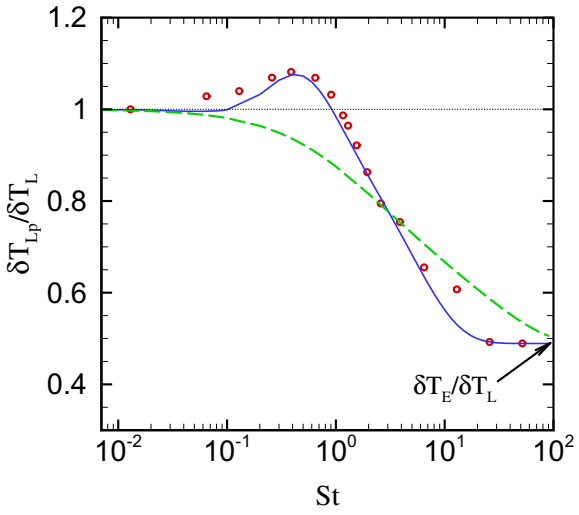

Figure 6. Variation of $\delta T_{Lp}/\delta T_L$ with particle Stokes number St, where the cutoff location is at $\eta k_c = 0.284$, $St \equiv \tau_p/\delta T_E$. Circles: FDNS result; solid line: equation (31); dashed line: the model $\delta T_{Lp}/\delta T_E = 1 - (1-\beta)/(1+St)^{0.4(1+0.01St)}$ proposed by Wang and Stock [11] where the timescales at full-scale, T_L and T_E, are replaced with those at SGS, δT_L and δT_E, respectively and $\beta = \delta T_L/\delta T_E = 2.26$; dotted line: $\delta T_{Lp} = \delta T_L$.

where $\beta = \delta T_L/\delta T_E$ which can be estimated using equations (28) and (29). η in LES is calculated using equation (27) with the total dissipation rate ε calculated using the SGS eddy viscosity model,

$$\varepsilon = 2\int_1^{k_c} [\nu + \nu_e(k|k_c)]k^2 E(k)\,\mathrm{d}k. \tag{32}$$

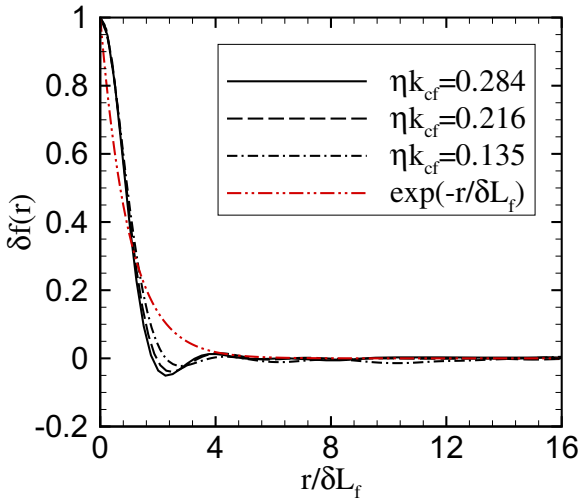

Figure 7. Normalized SGS longitudinal fluid spatial velocity correlation at different cutoff locations. The abscissa has been normalized by the longitudinal integral scale δL_f.

Equation (31) was optimized with the results from several cutoff locations, noting that both δT_{L} and δT_{E} also depend on k_{c}. It captures all the main characteristics of the dependence of δT_{Lp} on St and k_{c}. It is worth pointing out that the first term in the brackets represents that the magnitude of the convexity near $St = 0.5$ depends on the filter width ηk_{c}.

3.3. The elliptic model for the subgrid scale timescale seen by heavy particles under gravity

Under gravity, $\delta R_{\mathrm{L}p,ij}(\tau)$ and the timescale $\delta T_{\mathrm{L}p,ij}$ are anisotropic even in isotropic turbulent flows due to the drift velocity. The cross trajectory effect makes $\delta R_{\mathrm{L}p,ij}(\tau)$ decorrelate more rapidly in the direction of the drift velocity than in the case without drift velocity. In order to relate $\delta R_{\mathrm{L}p,ij}(\tau)$ to the statistics of SGS fluid turbulence, we shall extend the work of Csanady [14] and Wang and Stock [11] to transfer $\delta R_{\mathrm{L}p,ij}(\tau)$ from SGS temporal correlation to SGS spatial correlation when the drift velocity increases from 0 to ∞ in the context of LES. $\delta R_{\mathrm{L}p,ij}(\tau)$ in the direction of gravity can be approximately expressed using an exponential function

$$\delta R_{\mathrm{L}p,11}(\tau) = \exp\left(-\frac{\tau}{\delta T_{\mathrm{L}p,11}}\right). \tag{33}$$

The SGS longitudinal correlation function $\delta f(r)$ is defined as

$$\delta f(r) = \frac{\langle u_x'(x_0, y_0, z_0) u_x'(x_0 + r, y_0, z_0)\rangle}{\langle (u_x')^2(x_0, y_0, z_0)\rangle}. \tag{34}$$

The normalized SGS longitudinal correlations at different cutoff locations are plotted in figure 7. As the first-order approximation, we use an exponential relation to represent $\delta f(r)$ in the SGS flow field

$$\delta f(r) = \exp\left(-\frac{r}{\delta L_f}\right). \tag{35}$$

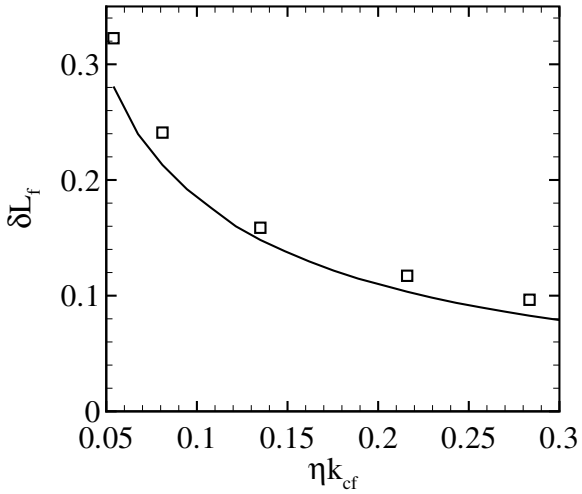

Figure 8. Variation of the SGS longitudinal integral scale with the filter width. Solid line: theoretical equation (39); squares: DNS result using equation (36) at different cutoff locations.

The abscissa in figure 7 has been normalized by the longitudinal integral scale δL_f which is defined as

$$\delta L_f \equiv \int_0^\infty \delta f(r)\,\mathrm{d}r. \tag{36}$$

By extending the relation $L_f = \left(\pi \big/ 2u_{\mathrm{rms}}^2\right) \int_0^\infty \left(E(k) \big/ k\right) \mathrm{d}k$ for the full-scale flow field in an isotropic turbulent flow into the SGS case [16], we can obtain

$$\delta L_f = \frac{\pi}{2u_{\mathrm{rms}}'^2} \int_{k_c}^\infty \frac{E(k)}{k}\mathrm{d}k, \tag{37}$$

where the SGS rms turbulent velocity u'_{rms} can be obtained from the 3D energy spectrum

$$u'_{\mathrm{rms}} = \frac{2}{3}\int_{k_c}^\infty E(k)\mathrm{d}k. \tag{38}$$

Introducing the energy spectrum $E(k) = C_{\mathrm{K}}\varepsilon^{2/3}k^{-5/3}$ in equations (37) and (38), we can obtain

$$\delta L_f = \frac{3}{10}\frac{\pi}{k_c}. \tag{39}$$

The comparison of equations (39) and (36) using DNS data is shown in figure 8. We can observe that the computational results and the theoretical formula are consistent with each other. Thus we can use equation (39) to estimate the necessary parameter, the lengthscale of the SGS motion, δL_f in the closure equations (46) and (47) for the SGS-SDE model.

The SGS transverse correlation function $\delta g(r)$ is defined as

$$\delta g(r) = \frac{\langle u'_y(x_0, y_0, z_0)u'_y(x_0+r, y_0, z_0) + u'_z(x_0, y_0, z_0)u'_z(x_0+r, y_0, z_0)\rangle}{\langle (u'_y)^2(x_0, y_0, z_0) + (u'_z)^2(x_0, y_0, z_0)\rangle}. \tag{40}$$

For an isotropic and incompressible turbulent flow, since the continuity equation $\mathbf{k}\cdot\hat{\mathbf{u}}=0$ holds for every wavenumber $\mathbf{k}$ in the spectral space, the SGS transverse correlation function $\delta g(r)$ can be obtained using the continuity relation

$$\delta g(r)=\delta f(r)+\frac{r}{2}\frac{\mathrm{d}(\delta f(r))}{\mathrm{d}r}. \tag{41}$$

Using equations (35) and (41), we can obtain

$$\delta g(r)=\left(1-\frac{r}{2\delta L_f}\right)\exp\left(-\frac{r}{\delta L_f}\right). \tag{42}$$

With equations (33), (35) and (42) for $\delta R_{\mathrm{L}p,11}(\tau)$, $\delta f(r)$ and $\delta g(r)$ respectively, we shall consider the SGS fluid velocity correlation seen by heavy particles $R_{\mathrm{L}p,ij}(\tau)$ under gravity.

The mean spatial displacement parallel to the direction of gravity is $r=\langle w\rangle\,\tau$ in the time interval τ for a heavy particle settling at a mean speed $\langle w\rangle$, which can be obtained from equation (11) if we neglect the effects of preferential sweeping on particle settling [18, 63]. This displacement leads to $\delta f(r)$, a decorrelation in space. As stated by Csanady [14], in the limiting case of $\delta L_f/\langle w\rangle \ll \min(\delta T_{\mathrm{L}},\delta T_{\mathrm{E}})$, we have $\delta R_{\mathrm{L}p,11}(\tau)=\delta f(\langle w\rangle\,\tau)$ parallel to the direction of gravity and $\delta R_{\mathrm{L}p,22}(\tau)=\delta R_{\mathrm{L}p,33}(\tau)=\delta g(\langle w\rangle\,\tau)$ perpendicular to the direction of gravity.

In a general situation, both the inertia and the drift velocity are not zero, and the two effects can be included in $\delta R_{\mathrm{L}p,11}(\tau)$ by extending the elliptic hypothesis of Csanady [14] into the SGS case that $\delta R_{\mathrm{L}p,11}(\tau)$ is a constant on the ellipse

$$\frac{\tau^2}{(\delta T_{\mathrm{Lp}})^2}+\frac{(\langle w\rangle\,\tau)^2}{(\delta L_f)^2}=\text{const.} \tag{43}$$

Equation (43) can be also derived from the elliptic model for Lagrangian time correlation, as done by He *et al* [64]. $\delta R_{\mathrm{L}p,11}(\tau)$ can be formally expressed as a Taylor series in terms of space and time separations, where the particle separations can be further expanded as a power series of time delay. The first-order approximation gives the Taylor frozen-flow model and the second-order one recovers the above elliptic model. Equation (43) makes a smooth transition of $\delta R_{\mathrm{L}p,11}(\tau)$ from the SGS temporal correlation to the SGS spatial correlation when $\langle w\rangle$ changes from 0 to ∞. If replacing $r/\delta L_f$, r with $\tau\sqrt{1/\delta T_{\mathrm{Lp}}^2+\langle w\rangle^2/\delta L_f^2}$ and $\langle w\rangle\,\tau$ in equations (35) and (42), respectively, we can obtain the SGS correlations seen by heavy particles in the gravitational direction $\delta R_{\mathrm{L}p,11}(\tau)$ and perpendicular to the gravitational direction $\delta R_{\mathrm{L}p,22}(\tau)=\delta R_{\mathrm{L}p,33}(\tau)$, respectively,

$$\delta R_{\mathrm{L}p,11}(\tau)=\exp(-\tau_n), \tag{44}$$

$$\delta R_{\mathrm{L}p,22}(\tau)=\left(1-\frac{\langle w\rangle\,\tau}{2\delta L_f}\right)\exp(-\tau_n), \tag{45}$$

where $\tau_n=\tau\sqrt{1/\delta T_{\mathrm{Lp}}^2+\langle w\rangle^2/\delta L_f^2}$. Integrating equations (44) and (45), we can get SGS timescales along the direction of the drift velocity $\delta T_{\mathrm{L}p,11}$ and normal to the direction of the drift velocity $\delta T_{\mathrm{L}p,22}$ or $\delta T_{\mathrm{L}p,33}$, respectively,

$$\delta T_{\mathrm{L}p,11}=\int_0^\infty \delta R_{\mathrm{L}p,11}(\tau)\,\mathrm{d}\tau=\frac{1}{\sqrt{\frac{1}{\delta T_{\mathrm{Lp}}^2}+\frac{\langle w\rangle^2}{\delta L_f^2}}}, \tag{46}$$

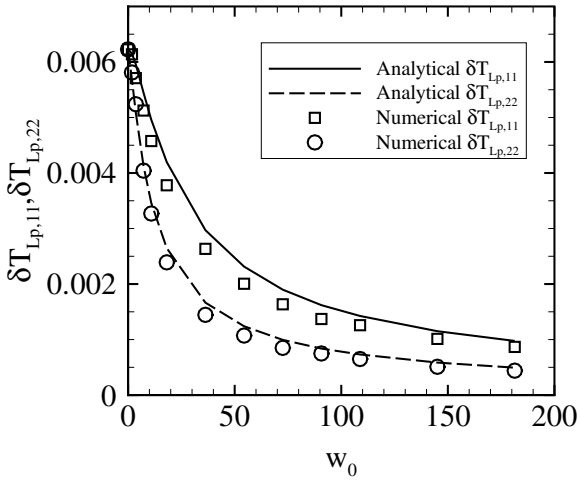

Figure 9. Variation of longitudinal and transverse SGS timescales $\delta T_{\mathrm{L}p,11}$ and $T_{\mathrm{L}p,22}$ or $T_{\mathrm{L}p,33}$with particle Stokes settling velocity w_0 for $St_{\mathrm{K}} = 0.5$ and filter width $\eta k_{\mathrm{c}} = 0.284$.

$$\delta T_{\mathrm{L}p,22} = \int_0^\infty \delta R_{\mathrm{L}p,22}(\tau)\,\mathrm{d}\tau = \frac{1}{\sqrt{\frac{1}{\delta T_{\mathrm{Lp}}^2} + \frac{\langle w\rangle^2}{\delta L_f^2}}} \left(1 - \frac{\langle w\rangle}{2\delta L_f} \frac{1}{\sqrt{\frac{1}{\delta T_{\mathrm{Lp}}^2} + \frac{\langle w\rangle^2}{\delta L_f^2}}}\right). \tag{47}$$

We compare the analytical results of equations (46) and (47) with our numerical results of drift velocity in figure 9. It is shown that the proposed formulae fit the numerical results well. With increasing drift velocity, $\delta T_{\mathrm{L}p,11}$ decreases due to the crossing trajectory effect (solid line and squares) and the continuity effect further reduces $\delta T_{\mathrm{L}p,22}$ or $\delta T_{\mathrm{L}p,33}$ (dashed line and circles). In the limit of very large drift velocities, $\langle w\rangle \to \infty$, $\delta T_{\mathrm{L}p,22} \to 0.5\delta T_{\mathrm{L}p,11}$.

To consider the anisotropy due to gravity, we can express the coefficient C_i on the right-hand side of equation (12) as [58]

$$C_i = C_1 b_i + \tfrac{2}{3}(b_i - 1), \tag{48}$$

where $b_i = \delta T_{\mathrm{Lp}}/\delta T_{\mathrm{L}p,ii}$ ($i = 1$ and 2 or 3) and C_1 can be expressed as follows when we consider the inertial effects

$$C_1 = \frac{C_0\beta}{\left\{(0.444 - 0.7\eta k_{\mathrm{c}})\exp\left\{-\left[\ln\left(\frac{St}{0.5}\right)\right]^2\right\} + 1 \; -(1-\beta)\exp\left(-\frac{St}{5.15}\right)\right\}}, \tag{49}$$

where $C_0 = 2.1$ in FDNS and $C_0 = 6.0$ in real LES to take into account the over-correlative flow structures due to the SGS model error. When the Stokes number is very small and there is no drift velocity, $C_1 = C_0$, $b_i = 1$, thus C_i reduces to C_0 for fluid particles [62].

We shall summarize the SGS-SDE model given by equation (12) where the SGS timescale $\delta T_{\mathrm{L}p,11}$ is given by equation (46), $\delta T_{\mathrm{L}p,22}$ and $\delta T_{\mathrm{L}p,33}$ are given by equation (47) where δL_f is given by equation (39), $\langle w\rangle$ is given by equation (11), δT_{Lp} is given by equation (31) where β is given by equations (28) and (29). The coefficient C_i is given by equations (48) and (49). The SGS-SDE (12) is then closed. We shall validate this model by predicting the particle relative dispersion in the next section.

4. Large-eddy simulation of two-particle relative dispersion

4.1. Validation of the subgrid scale-stochastic differential equation model by comparison with direct numerical simulation

The relative dispersion of heavy particles is very important in turbulent transport and mixing in many industrial and natural flows. The correlations in local turbulent structures are responsible for the superdiffusive separation of heavy particles [5, 65]. In isotropic turbulence, the two-particle relative dispersion is mainly dominated by small-scale motions which cannot be resolved in conventional LES. Thus prediction of two-particle relative dispersion poses a challenge for the LES method. In LES, SGS fluid velocity and SGS turbulent structures are removed due to the filtering operation, and the SGS eddy viscosity model is usually over-dissipative and it also alters the spatial-time correlations of the resolved motions [26]. Thus, the relative dispersion of inertial particles might be affected by the SGS motions.

In this subsection, we shall validate the proposed closure for the SGS-SDE model (equation (12)) to consider the effects of SGS motions on two-particle relative dispersion *with an initial separation in the inertial subrange* using FDNS and LES respectively. The separation between two particles in time is $\mathbf{R}(t) \equiv \mathbf{x}_{p,2}(t) - \mathbf{x}_{p,1}(t)$, where $\mathbf{x_{p,2}(t)}$ and $\mathbf{x_{p,1}(t)}$ are the positions of two particles. The relative dispersion is defined as $\langle \delta\mathbf{R}(t, R_0) \cdot \delta\mathbf{R}(t, R_0) \rangle$ where $\delta\mathbf{R}(t) = \mathbf{R}(t) - \mathbf{R}(t=0)$ is the vectorial separation increment and the initial separation $R_0 = |\mathbf{R}(t=0)|$. For fluid particles with an initial separation in the inertial subrange, $\eta \ll R_0 \ll L_f$ and $t \ll T_\mathrm{E}$, the relative dispersion has two regimes, that is, the Batchelor regime and the Richardson regime, respectively,

$$\langle \delta\mathbf{R}(t, R_0) \cdot \delta\mathbf{R}(t, R_0) \rangle = \begin{cases} \dfrac{11}{3} C_0 R_0^2 \left(\dfrac{t}{t_0}\right)^2, & t \ll t_0 \equiv \left(\dfrac{R_0^2}{\varepsilon}\right)^{1/3}, \\ g_\mathrm{R} \varepsilon t^3, & t_0 \ll t \ll T_\mathrm{E}, \end{cases} \tag{50}$$

where L_f is the integral lengthscale, T_E is the large-eddy turnover time, $T_\mathrm{E} = L_f / u_\mathrm{rms} = (L_f^2/\varepsilon)^{1/3}$, g_R is the Richardson constant and $C_0 = 2.1$. The Batchelor regime has been observed numerically or experimentally, while the existence of the Richardson regime has not been well established [5, 65]. The Batchelor regime was also experimentally observed for heavy particles. The heavy particles initially separate faster than fluid particles [65].

When the flow reaches a stationary state, 2×10^5 pairs of particles with an initial separation of $R_0 = 20\eta = 0.27$ are released into the flow field. The initial particle velocities are set to be the fluid velocities at the individual particle position. The life time of an eddy at scale R_0 is $t_0 = 0.0268$ and its ratio to the large-eddy turnover time is $T_\mathrm{E}/t_0 = 1.86$ for the simulated flow at a modest Reynolds number. In LES, the resolution of 32^3 is used. In FDNS, the cutoff wavenumber is $k_\mathrm{c} = 10$. The SGS lengthscale estimated using equation (39) in LES and FDNS is about $\delta L_f = 0.09$, much smaller than the initial separation, $R_0 = 0.27$. In figures 10–13, the solid line denotes the result obtained from DNS, the short dashed line denotes the result from FDNS, the long dashed line denotes the result from LES, the dash-dot-dotted line denotes the result from FDNS with the SGS-SDE model and the dash-dotted line denotes the result from LES with the SGS-SDE model. Please note that the dashed line for FDNS and the dash-dotted line for LES with SGS-SDE model almost collapse in figure 13(b). One can observe that both FDNS and LES under-predict the relative dispersion of heavy particles due to missing fluctuating SGS fluid motions. Another observation is that LES under-predicts the

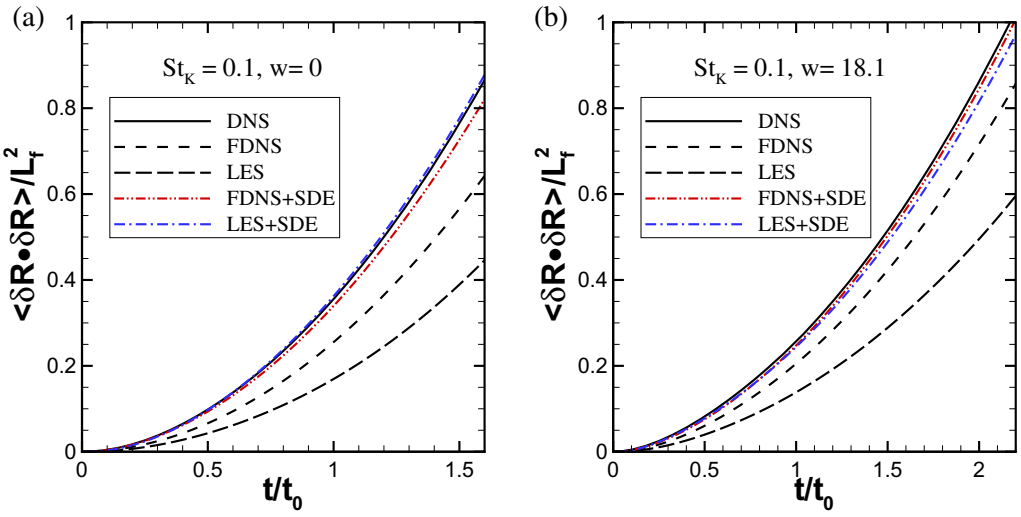

Figure 10. Comparison of the results from DNS, FDNS, LES, FDNS plus SDE and LES plus SDE at Stokes number $St_K = 0.1$. (a) $St_K = 0.1$, $w = 0$ and (b) $St_K = 0.1$, $w = 18.1$.

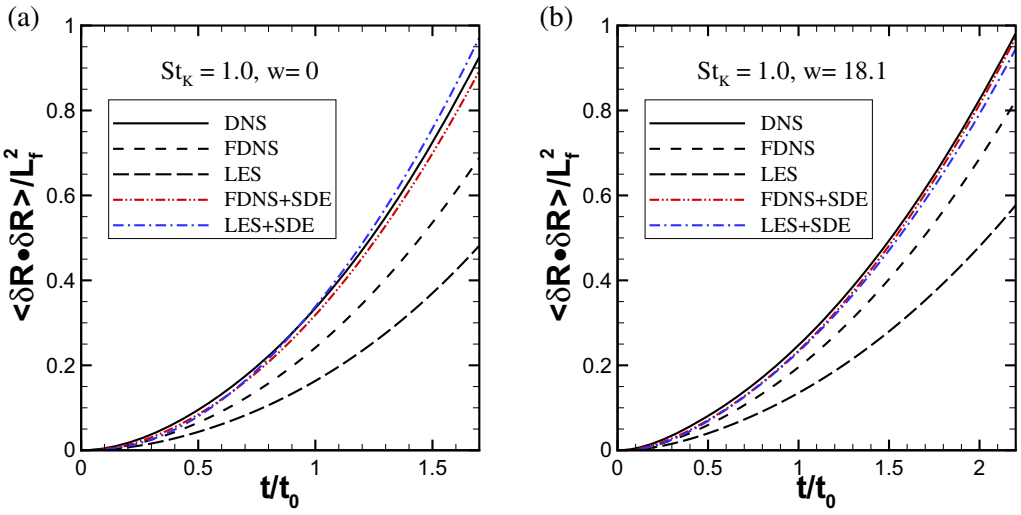

Figure 11. Comparison of the results from DNS, FDNS, LES, FDNS plus SDE and LES plus SDE at Stokes number $St_K = 1.0$. (a) $St_K = 1.0$, $w = 0$ and (b) $St_K = 1.0$, $w = 18.1$.

relative dispersion even lower than FDNS. This is due to the SGS model error. The SGS eddy viscosity model used to close the filtered Navier–Stokes equations (4) makes the fluid field more correlative than that in FDNS [26], thus, particles separate slower in LES flow field than in FDNS flow field. Therefore, a larger value of the coefficient $C_0 = 6.0$ in equation (49) is needed in the LES plus SGS-SDE model to recover the effects of SGS motion on particle separation. It means that more strongly modeled SGS perturbations are needed in the real LES plus SGS-SDE model than in the FDNS plus SGS-SDE model to separate particle pairs. The observations show that the proposed SGS-SDE model can improve the prediction of relative dispersion in all cases at Stokes numbers $St_K = 0.1$, 1.0, 2.0 and 3.0 both with and without the force of gravity,

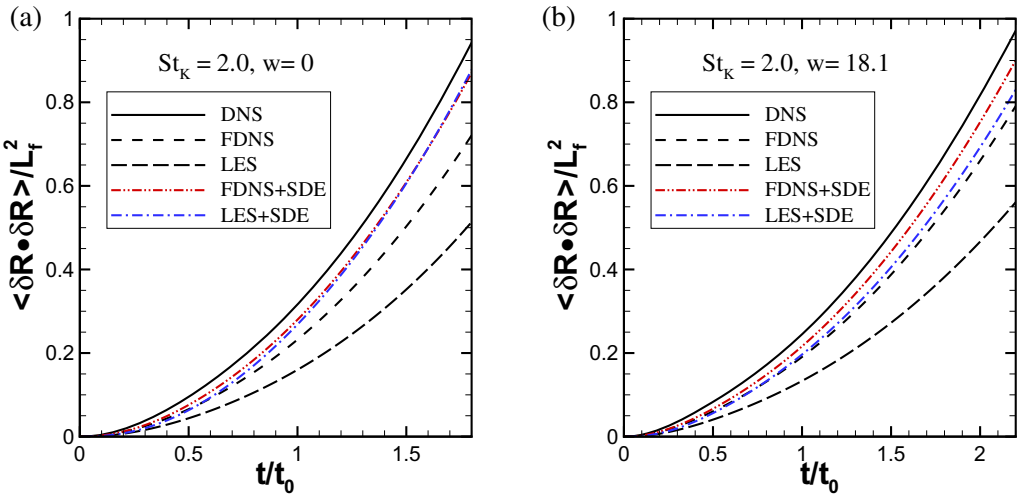

Figure 12. Comparison of the results from DNS, FDNS, LES, FDNS plus SDE and LES plus SDE at Stokes number $St_K = 2.0$. (a) $St_K = 2.0$, $w = 0$ and (b) $St_K = 2.0$, $w = 18.1$.

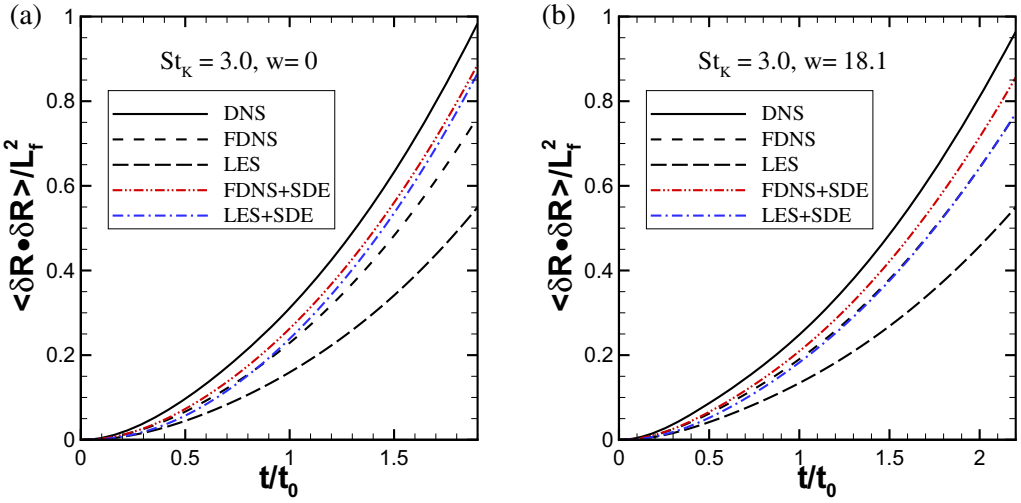

Figure 13. Comparison of the results from DNS, FDNS, LES, FDNS plus SDE and LES plus SDE at Stokes number $St_K = 3.0$. In (b) the dashed line for FDNS and the dash-dotted line for LES plus SDE almost collapse. (a) $St_K = 3.0$, $w = 0$ and (b) $St_K = 3.0$, $w = 18.1$.

respectively. In the cases with gravity, the drift velocity is 18.1, which is comparable to the rms turbulent fluctuating velocity. The drift velocity reduces the relative dispersion of heavy particles in all cases. The result is consistent with the results of EIMaihy and Nicolleau [66] in which heavy particles disperse in a flow field based on kinematic simulation. We can also notice that with increasing Stokes number, the performance of the SGS-SDE model for heavy particles with larger Stokes number decreases. This is physical since heavy particles with larger Stokes numbers are awkward to respond to recovered SGS motions by the SGS-SDE model with increasing inertia.

4.2. Assessment of the subgrid scale-stochastic differential equation model by comparing with the approximate deconvolution methods

In addition to the SGS-SDE model discussed above, SGS models based on fractal interpolation and the ADM were used to model the effects of SGS turbulence on the statistics of fluid and particle velocities and particle concentration in channel flows by Marchioli *et al* [27]. It was shown that the two-dimensional fractal interpolation is inefficient since the reconstructed fluid signals vary rather smoothly in space. An improvement in the prediction of wall-normal particle concentration was obtained using the ADM.

In this subsection, we shall compare the performance of the SGS-SDE model with the ADM on relative particle dispersion in isotropic turbulence. The main principle of the ADM is to approximate the inverse of a smooth filter $\hat{G}^{-1}(k)$ by a truncated series of the filter $\hat{G}(k)$,

$$\hat{G}^{-1}(k) \simeq \sum_{n=0}^{N} \left(I - \hat{G}(k)\right)^n, \tag{51}$$

where I is the identity operator. According to Stolz and Adams [33], $N = 5$ is sufficient. Therefore, we can obtain the approximation of the inverse of a smooth filter, $\hat{G}^{-1}(k)$, when $N = 5$,

$$\hat{G}^{-1}(k) \simeq 6 - 15\hat{G}(k) + 20\hat{G}^2(k) - 15\hat{G}^3(k) + 6\hat{G}^4(k) - \hat{G}^5(k). \tag{52}$$

Using equation (52), we can obtain the improved fluid velocity $\hat{u}^*(k,t)$ by

$$\begin{aligned} u^*(k,t) &= \hat{G}^{-1}(k) * \hat{\bar{u}}(k,t) \\ &\simeq 6\hat{\bar{u}}(k,t) - 15\hat{\bar{\bar{u}}}(k,t) + 20\hat{\bar{\bar{\bar{u}}}}(k,t) - 15\hat{\bar{\bar{\bar{\bar{u}}}}}(k,t) + 6\hat{\bar{\bar{\bar{\bar{\bar{u}}}}}}(k,t) - \hat{\bar{\bar{\bar{\bar{\bar{\bar{u}}}}}}}(k,t), \end{aligned} \tag{53}$$

where the multiple bars over $\hat{u}$ denote repeated filtering, that is, $\hat{\bar{\bar{u}}}(k,t) = \hat{G}(k,t) * \hat{\bar{u}}(k,t)$, $\hat{\bar{\bar{\bar{u}}}}(k,t) = \hat{G}(k,t) * \hat{\bar{\bar{u}}}(k,t)$, ..., and $\hat{\bar{u}}(k,t)$ is the resolved velocity from LES. We choose the 3D Gaussian and top-hat filters in this study and they are defined as follows:

$$\hat{G}(\mathbf{k}) = \begin{cases} \exp\left(-\dfrac{|\mathbf{k}|^2 \Delta^2}{24}\right) & \text{if } |\mathbf{k}| < k_c, \\ 0 & \text{if } |\mathbf{k}| > k_c \end{cases} \tag{54}$$

and

$$\hat{G}(\mathbf{k}) = \begin{cases} \dfrac{\sin\left(\frac{1}{2}k_x\Delta\right)}{\frac{1}{2}k_x\Delta} \dfrac{\sin\left(\frac{1}{2}k_y\Delta\right)}{\frac{1}{2}k_y\Delta} \dfrac{\sin\left(\frac{1}{2}k_x\Delta\right)}{\frac{1}{2}k_z\Delta} & \text{if } |\mathbf{k}| < k_c, \\ 0 & \text{if } |\mathbf{k}| > k_c. \end{cases} \tag{55}$$

The one-dimensional Gaussian and top-hat filters and their inverses computed using equation (52) are shown in figure 14. We can observe that the two filters and their inverses are qualitatively similar and the inverse filters can increase the Fourier coefficients near the cutoff wavenumber ($k/k_c \approx 1$) by about 50%.

The function of the SGS-SDE model is to reconstruct the SGS fluid velocity along the trajectory of a heavy particle, while the ADM tends to improve the accuracy of the resolved

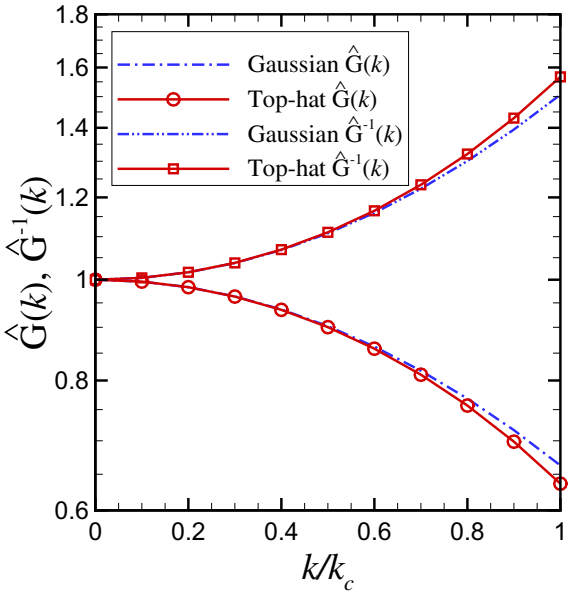

Figure 14. The one-dimensional Gaussian and top-hat filters and their approximate inverses.

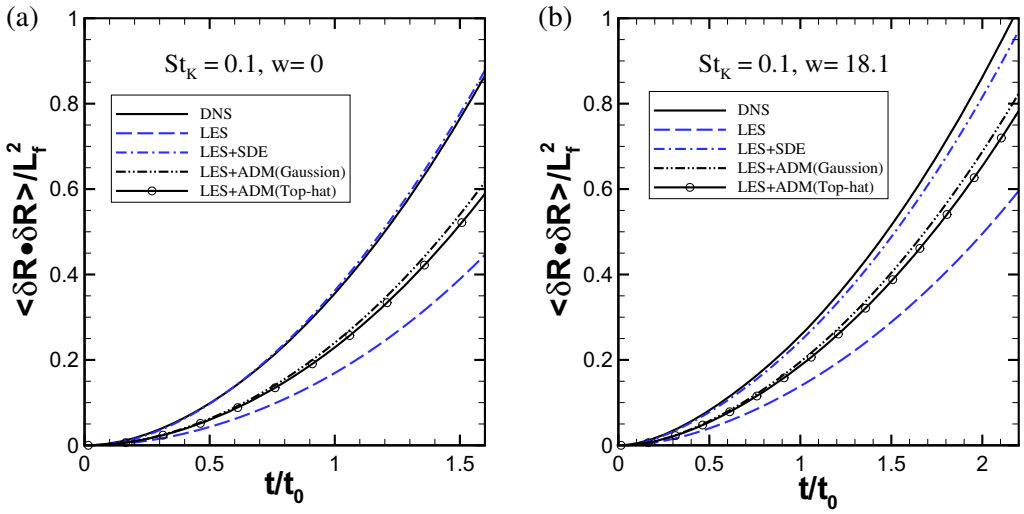

Figure 15. Comparison of LES plus SDE and LES plus ADM at Stokes number $St_K = 0.1$. (a) $St_K = 0.1$, $w = 0$ and (b) $St_K = 0.1$, $w = 18.1$.

scales near the cutoff wavenumber in LES but not to recover the scales smaller than the filter width. The performances of the SGS-SDE model and the ADM on relative dispersion thus might depend on particle inertia. This is because the motions of particles with small Stokes numbers are sensitive to the fluctuating SGS velocity, and the motion of particles becomes less and less sensitive to the fluctuating SGS velocity with increasing Stokes number. Therefore, the SGS-SDE model improves the relative dispersion of particles with small Stokes numbers and the ADM improves the relative dispersion of particles with modest Stokes numbers. This tendency

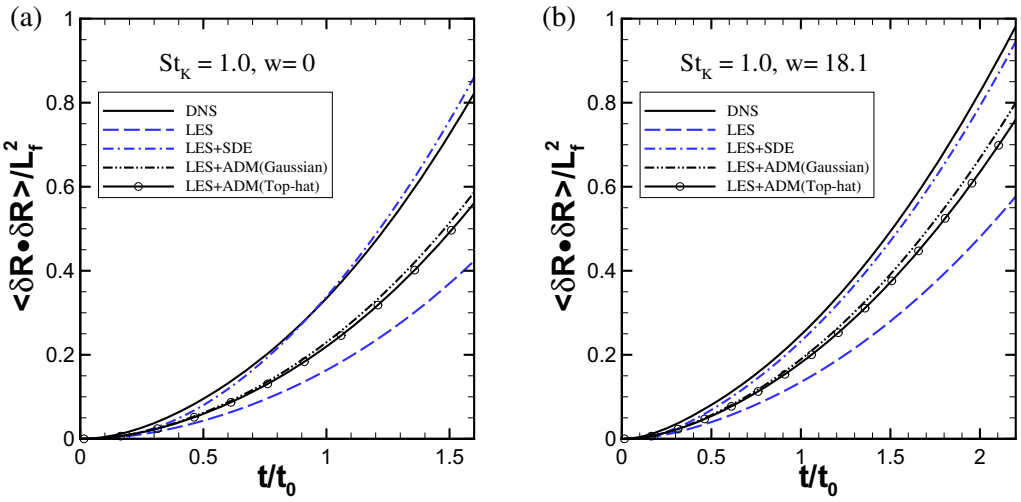

Figure 16. Comparison of LES plus SDE and LES plus ADM at Stokes number $St_K = 1.0$. (a) $St_K = 1.0$, $w = 0$ and (b) $St_K = 0.1$, $w = 18.1$.

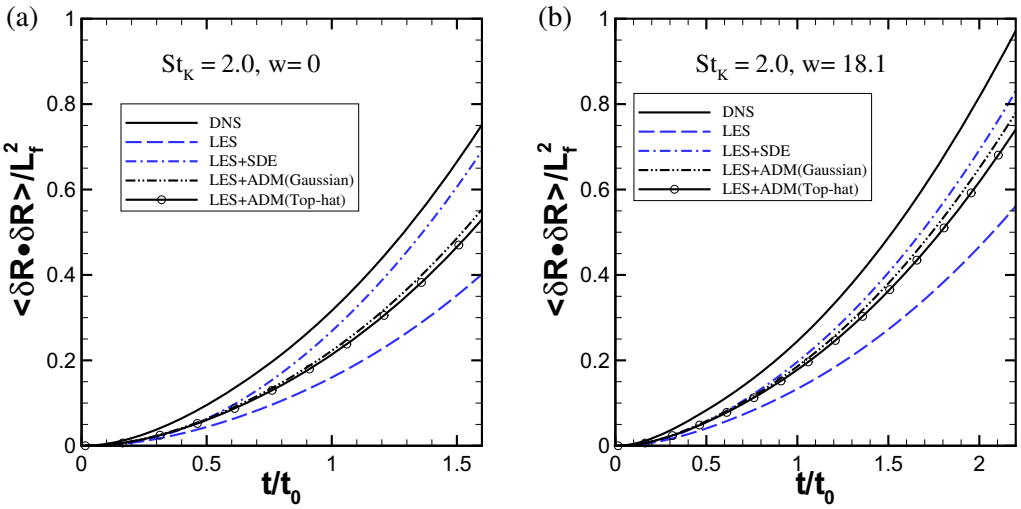

Figure 17. Comparison of LES plus SDE and LES plus ADM at Stokes number $St_K = 2.0$. (a) $St_K = 2.0$, $w = 0$ and (b) $St_K = 2.0$, $w = 18.1$.

is demonstrated through figures 15–18, where both the SGS-SDE model and AMD can improve the prediction of relative dispersion for all Stokes numbers, but the extent of improvement varies for particles with different Stokes numbers. In figures 15 and 16, the SGS-SDE model performs well while the ADM performs modestly at $St_K = 0.1$ and 1.0. In figure 17, both the SGS-SDE model and the ADM perform modestly for particles with $St_K = 2.0$, while the ADM performs well but the SGS-SDE model performs modestly for particles with $St_K = 3.0$ in figure 18. Another observation in figures 15–18 is that the Gaussian filter and the top-hat filter perform similarly. This is expected from figure 14, where the Gaussian inverse filter and top-hat inverse filter are very similar.

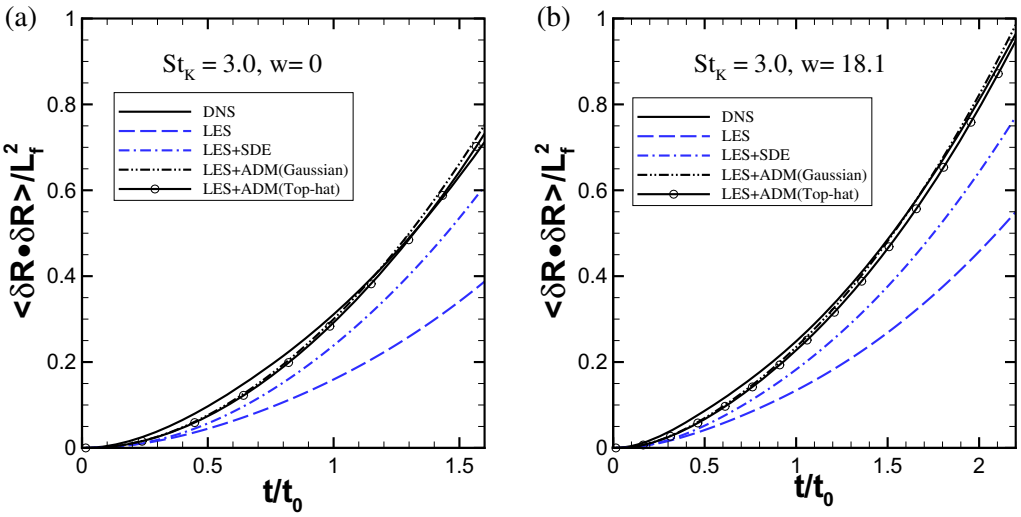

Figure 18. Comparison of LES plus SDE and LES plus ADM at Stokes number $St_K = 3.0$. (a) $St_K = 3.0$, $w = 0$ and (b) $St_K = 3.0$, $w = 18.1$.

5. Conclusions and future work

Relative dispersion of heavy particles is very important for turbulent transport and mixing and it is mainly determined by small-scale motions in isotropic turbulence which are absent in conventional LES. Therefore, prediction of turbulent relative dispersion raises a new challenge for the LES method. In this paper, we propose the use of an SGS-SDE model to represent the effects of the SGS eddies on the relative dispersion in LES. Although the stochastic Langevin equation is not new, how to close the equation which accounts for filter width, particle inertia and gravity is important in the context of LES. The main objective of this paper is to provide the SGS timescale seen by heavy particles for the SGS-SDE model. For this purpose, the physics of the interaction between heavy particles and the SGS turbulence obtained by FDNS has to be explored.

The *new physical findings* include:

1. The timescales of SGS velocity fields are not only quantitatively but also qualitatively different from the ones of full-scale velocity fields. The SGS Eulerian timescale δT_E is shorter than its Lagrangian counterpart δT_L because the SGS eddies are contained and convected by large-scale eddies in the flow. Their ratio $\beta = \delta T_L/\delta T_E$, a necessary parameter for the closure, is larger than unity and changes with the filter widths.
2. In the absence of gravity, the SGS timescale δT_{Lp} non-monotonically varies with particle Stokes number from the SGS Lagrangian timescale to the SGS Eulerian timescale with a maximum at Stokes number $St = \tau_p/\delta T_E$ near 0.5 due to the inertial bias between the fluid and heavy particles.
3. In the presence of gravity, a similarity law exists between the SGS Lagrangian correlation function seen by a heavy particle within a time-delay τ and the SGS spatial correlation function with the displacement $\langle w\rangle\tau$ of a heavy particle. To combine the effects of particle inertia and gravity on the SGS timescale seen by particles, a nonlinear elliptic model is first extended into the SGS flow fields to analytically derive the SGS timescale seen by heavy particles.

4. The crossing trajectory effect due to gravity reduces $\delta T_{\mathrm{L}p,11}$ with increasing settling velocity and the continuity effect further reduces $\delta T_{\mathrm{L}p,22}$ or $\delta T_{\mathrm{L}p,33}$.
5. Gravity tends to reduce the relative dispersion of heavy particles in isotropic turbulent flows.

The nonlinear model for the SGS timescale seen by particles is then used to close the SGS-SDE model for LES and FDNS. It is validated against DNS of relative dispersion. The proposed model can improve the prediction of relative dispersion with *an initial separation in the inertial subrange* at different Stokes numbers with and without gravitational force, respectively. Furthermore, the assessment of the relative performances of the SGS-SDE model and the ADM is carried out. We found that the SGS-SDE model is suitable for particles with small Stokes numbers, $St_{\mathrm{K}} < 2$, while the ADM is more suitable for particles with modest Stokes numbers, $St_{\mathrm{K}} > 2$.

The LES prediction of other quantities related to particle separations such as the radial distribution function and the mean radial relative velocity between particles with the SGS-SDE model needs to be investigated in the future. In turbulent channel flows, the SGS timescale seen by particles changes with the distance from the wall due to the presence of strong shear rates and high flow anisotropy in the near-wall region [8, 27, 67]. The corresponding problem that should be studied is the effects of the shear rate on the SGS timescale seen by heavy particles.

Acknowledgments

This work is supported by NSFC under grant numbers 11072247, 11021262 and 1123201, and NSAF under number U1230126. We thank Professor Lian-Ping Wang at the University of Delaware, USA for the discussions during the work of this paper. Part of the work was done during the 'New Directions in Turbulence' 2012 Program at the Kavli Institute for Theoretical Physics China (KITPC) at the Chinese Academy of Sciences (CAS). We would like to thank the two anonymous referees for their very constructive and insightful suggestions and comments on the original manuscript.

References

[1] Crowe C T, Sommerfeld M and Tsuji Y 1998 *Multiphase Flows with Droplets and Particles* (Boca Raton, FL: CRC Press)
[2] Devenish B J *et al* 2012 *Q. J. R. Meteorol. Soc.* **138** 1401–29
[3] Gidaspow D 1994 *Multi-Phase Flow and Fluidization: Continuum and Kinetic Theory Descriptions* (Boston, MA: Academic)
[4] Xiang Q G *et al* 2012 *Chem. Eng. Sci.* **71** 422–30
[5] Bourgoin M, Ouellette N, Xu H T, Berg J and Bodenschatz E 2006 *Science* **311** 835–8
[6] Toschi F and Bodenschatz E 2009 *Annu. Rev. Fluid Mech.* **41** 375–404
[7] Salazar J P L C and Collins L R 2009 *Annu. Rev. Fluid Mech.* **41** 405–32
[8] Pitton E, Marchioli C, Lavezzo V, Soldati A and Toschi F 2012 *Phys. Fluids* **24** 073305
[9] Simonin O, Deutsch E and Minier J P 1993 *Appl. Sci. Res.* **51** 275–83
[10] Chibbaro S and Minier J P 2008 *J. Aerosol Sci.* **39** 555–71
[11] Wang L P and Stock A D 1993 *J. Atmos. Sci.* **50** 1897–913
[12] Oesterlé B and Zaichik L 2006 *Int. J. Multiph. Flow* **32** 838–49
[13] Pozorski J and Minier J P 1998 *Int. J. Multiph. Flow* **24** 913–45

[14] Csanady G T 1963 *J. Atmos. Sci.* **20** 201–8
[15] He Z, Liu Z, Chen S, Weng L and Zheng C 2005 *Acta Mech. Sin.* **21** 112–20
[16] Fede P and Simonin O 2006 *Phys. Fluids* **18** 045103
[17] Jung J, Yeo K and Lee C 2008 *Phys. Rev.* E **77** 016307
[18] Wang L P and Maxey M R 1993 *J. Fluid Mech.* **256** 27–68
[19] Sundaram S and Collins L R 1997 *J. Fluid Mech.* **335** 75–109
[20] Moin P and Mahesh K 1998 *Annu. Rev. Fluid Mech.* **30** 539–78
[21] Germano M, Piomelli U, Moin P and Cabot W H 1991 *Phys. Fluids* **3** 1760–5
[22] Pope S B 2000 *Turbulent Flows* (London: Cambridge University Press)
[23] Li J C 2001 *Acta Mech. Sin.* **17** 289–301
[24] Yamamoto Y, Potthoff M, Tanka T, Kajishima Y and Tsuji Y 2001 *J. Fluid Mech.* **442** 303–34
[25] Sagaut P 2006 *Large Eddy Simulation for Incompressible Flows: An Introduction* 3rd edn (Berlin: Springer)
[26] He G W, Rubinstein R and Wang L P 2002 *Phys. Fluids* **14** 2186–93
[27] Marchioli C, Salvetti M V and Soldati A 2008 *Phys. Fluids* **20** 040603
[28] Marchioli C, Salvetti M V and Soldati A 2008 *Acta Mech.* **201** 277–96
[29] Yang Y, He G W and Wang L P 2008 *J. Turbul.* **9** 1–24
[30] Zhang J, He G W and Lu L P 2009 *Acta Mech. Sin.* **25** 45–9
[31] Jin G D, He G W and Wang L P 2010 *Phys. Fluids* **22** 055106
[32] Bianco F, Chibbaro S, Marchioli C, Salvetti M V and Soldati A 2012 *Phys. Fluids* **24** 045103
[33] Stolz S and Adams N A 1999 *Phys. Fluids* **11** 1699–701
[34] Kuerten J G M and Verman A W 2005 *Phys. Fluids* **17** 011701
[35] Shotorban B and Mashayek F 2005 *Phys. Fluids* **17** 081701
[36] Kuerten J G M 2006 *Phys. Fluids* **18** 025108
[37] Hickel S, Adams N A and Domaradzki J A 2006 *J. Comput. Phys.* **213** 413–36
[38] Shotorban B, Zhang K K Q and Mashayek F 2007 *Int. J. Heat Mass Transfer* **50** 3728–39
[39] Shotorban B and Mashayek F 2006 *J. Turbul.* **7** 1–13
[40] Shotorban B and Mashayek F 2006 *Proc. IUTAM Symp. on Computational Multiphase Flow* ed S Balachandar and A A Prosperetti (Dordrecht: Springer) pp 373–80
[41] Fede P, Simonin O, Villedieu P and Squires K D 2006 *Proc. CTR Summer Program 2006* (Stanford: Stanford University)
[42] Berrouk A S, Laurence D, Riley J J and Stock D E 2007 *J. Turbul.* **8** 1–20
[43] Berrouk A S, Stock D E, Laurence D and Riley J J 2008 *Int. J. Multiph. Flow* **34** 916–23
[44] Pozorski J and Apte S V 2009 *Int. J. Multiph. Flow* **35** 118–28
[45] Bini M and Jones W P 2008 *J. Fluid Mech.* **614** 207–52
[46] Jin G D, He G W, Wang L P and Zhang J 2010 *Int. J. Multiph. Flow* **36** 432–7
[47] Pozorski J, Knorps M and Luniewski M 2011 *J. Phys.: Conf. Ser.* **333** 012014
[48] Geurts B J and Kuerten J G M 2012 *Phys. Fluids* **24** 081702
[49] Eswaran E and Pope S B 1988 *Comput. Fluids* **16** 257–78
[50] Chollet J P and Lesieur M 1981 *J. Atmos. Sci.* **38** 2747–57
[51] Chollet J P 1985 *Turbulent Shear Flows (Karlsruhe 1983)* vol 4, ed L J S Bradbury (Berlin: Springer) pp 62–72
[52] Yeung P K and Zhou Y 1997 *Phys. Rev.* E **56** 1746–52
[53] Ishihara T, Gotoh T and Kaneda Y 2009 *Annu. Rev. Fluid Mech.* **41** 165–80
[54] Sreenivasan K R 1995 *Phys. Fluids* **7** 2778–84
[55] Chasnov J R 1991 *Phys. Fluids* A **3** 188–200
[56] Maxey M R and Riley J J 1983 *Phys. Fluids* **26** 883–9
[57] Pope S B 1994 *Annu. Rev. Fluid Mech.* **26** 23–63
[58] Minier J P and Peirano E 2001 *Phys. Rep.* **352** 1–214
[59] Yeung P K 2001 *J. Fluid Mech.* **427** 241–74

[60] Du S, Sawford B L, Wilson J D and Wilson D J 1995 *Phys. Fluids* **7** 3083–90
[61] Sawford B L and Yeung P K 2011 *Phys. Fluids* **23** 091704
[62] Sheikhi M R H, Drozda T G, Givi P and Pope S B 2003 *Phys. Fluids* **15** 2321–37
[63] Ayala O, Rosa B, Wang L P and Grabowski W W 2008 *New J. Phys.* **10** 1–31
[64] He G W, Jin G D and Zhao X 2009 *Phys. Rev.* E **80** 066313
[65] Gibert M, Xu H T and Bodenschatz E 2010 *Europhys. Lett.* **90** 64005
[66] ElMaihy A and Nicolleau F 2005 *Phys. Rev.* E **71** 046307
[67] Wang B and Manhart M 2012 *Acta Mech. Sin.* **28** 595–604